

X-Ray Observation of the L1157 Dark Cloud Region with ASCA

Tae FURUSHO, Noriko Y. YAMASAKI, and Takaya OHASHI,

Department of Physics, Tokyo Metropolitan University, 1-1 Minami-Ohsawa,

Hachioji, Tokyo 192-0397

E-mail(TF): furusho@phys.metro-u.ac.jp

Yoshitaka SAITO

Institute of Space and Astronautical Science (ISAS),

3-1-1 Yoshinodai, Sagami-hara, Kanagawa 229-8510

and

Wolfgang VOGES

Max-Planck-Institut für Extraterrestrische Physik, D-85748, Garching, Germany

(Received ; accepted)

Abstract

ASCA observation of a region containing a Class 0 protostar, IRAS 20386+6751 in the L1157 dark cloud, has been carried out. The protostar was not detected, and the 95% upper limit to the luminosity depends on assumed N_{H} : $L_{\text{X}}(0.5 - 10 \text{ keV}) < 1.1 \times 10^{31} \text{ erg s}^{-1}$ for $N_{\text{H}} = 1 \times 10^{23} \text{ cm}^{-2}$. A Class I protostar in L1152, IRAS 20353+6742, in the same field was also undetected with the upper limit about three times as much as the L1157 level. Besides these non detections, nine new X-ray sources were detected and spectral analysis was performed for 4 sources. One object (AXJ 2038+6801) shows a hard spectrum with a temperature $kT \sim 8 \text{ keV}$ or a power-law photon index ~ 2.0 and absorbed with $N_{\text{H}} \sim 2 \times 10^{22} \text{ cm}^{-2}$. Another fainter one (AXJ 2036+6800) has a soft spectrum with most of the emission falling below 2 keV. We examine possible nature of these new X-ray sources based on their spectral properties.

Key words: Stars: pre-main-sequence — Stars: X-rays — Stars: individual (L1157) — X-rays: spectra — X-rays: sources

1. Introduction

Young stellar objects are mainly classified into 4 classes based on the slope of their spectral energy distribution (SED) at infrared to millimeter wavelength (André et al. 1993); Class 0 and I protostars, Class II classical T Tauri stars, and Class III weak-lined T Tauri Stars. Class 0 protostars are thought to be in an evolutionary stage prior to Class I and are still in an active accretion phase. The typical life time of Class 0 objects is estimated to be about 10^4 yr and the temperature derived by fitting the spectrum with a single black body model is less than 100 K. It is also known that well collimated CO outflows are associated with most of Class 0 protostars (Bachiller 1996). X-ray emission from Class I protostars has been discovered by ROSAT and ASCA satellites (Casanova et al. 1995, Koyama et al. 1996, Kamata et al. 1997, Ozawa et al. 1999); however, not all Class I protostars are X-ray emitters. Their spectra are harder than those of T Tauri Stars, and the X-ray emission sometimes shows time variability like solar flares. Class I objects detected with ASCA, for instance WL6 and EL29 in the ρ Ophiuchi dark cloud, indicate 2 – 10 keV luminosities in the low state to be 2.5 and 3.3×10^{30} erg s $^{-1}$, respectively (Kamata et al. 1997). Their spectra can be fitted with an absorbed thermal bremsstrahlung model with a temperature $kT \sim 2\text{--}3$ keV, and a hydrogen column density $N_{\text{H}} \sim 4 \times 10^{22}$ cm $^{-2}$. The mechanism of the X-ray emission from protostars, however, has not been clearly understood yet. Naively, it is likely that the release of kinetic energy or angular momentum of the accreting matter drives both the CO outflow and X-ray emission. Our motivation for this observation is to study in what evolutionary stage a protostar starts to emit X-rays. The X-ray emission from a Class 0 protostar, if detected, would provide useful clues to solve this important problem.

In the L1157 cloud, a well collimated CO outflow is found by Umemoto et al. (1992), which is driven by IRAS 20386+6751 with its low luminosity ($\approx 11L_{\odot}$) at a distance of 440 pc. The outflow extends over about 5' (~ 0.6 pc) and the dynamical time scale is estimated to be $2\text{--}3 \times 10^4$ yr. The mass of the central object is $\sim 0.2M_{\odot}$, lower than the estimated mass of the surrounding envelope $M_{\text{env}} \sim 3M_{\odot}$ (Gueth et al. 1997). The fact that most of the mass is in the envelope suggests that this young object – hereafter called “L1157-mm” – is still in main accretion phase. The SED of the IRAS source, $F_{\nu}(100 \mu\text{m})/F_{\nu}(60 \mu\text{m}) = 4.0$, also shows the characteristics of the Class 0 objects (Tafalla, Bachiller 1995). Although ASCA has observed several tens of Class 0 protostars, no clear X-ray emission has been detected from them. Most of the objects lie in crowded regions, making a clear identification difficult even if there was an indication of X-ray emission. Since L1157-mm is relatively isolated, we have little ambiguity in

determining the origin of X-ray emission to be whether from L1157-mm or from others with the ASCA data.

The GIS field of view includes a Class I protostar in the L1152 dark cloud, which has been identified as IRAS 20353+6742. The coordinate of IRAS 20353+6742 is (R.A., Decl.)_{J2000} = (20^h35^m46^s, 67°53'2''), and it is about 21' away from L1157-mm. This source also shows the CO bipolar outflow detected by Bontemps et al. (1996), and the envelope mass is estimated to be 0.05 M_{\odot} . The distance is the same as that of L1157-mm and the bolometric luminosity is 3.3 L_{\odot} (Myers et al. 1987).

2. Observation

We observed L1157-mm with the ASCA satellite (Tanaka et al. 1994) on 1998 September 5 for a net exposure time of about 60 ks. The coordinate of L1157-mm position is (R.A., Decl.)_{J2000} = (20^h39^m6^s, 68°2'13''). ASCA has four identical X-ray telescopes (XRT) which collect incident X-rays onto two Solid-state Imaging Spectrometers (SIS0, SIS1) and two Gas Imaging Spectrometers (GIS2, GIS3). The field of view of each SIS is 11' × 11' and the covered energy range is 0.4 – 10 keV with an energy resolution of about 160 eV (FWHM) at 6 keV (Burke et al. 1991). The GIS instrument has a field of view of 40' diameter and covers the energy range from 0.7 keV to 10 keV with an energy resolution of 0.5 keV (FWHM) at 5.9 keV (Ohashi et al. 1996). During this observation, the SIS was operated in the 1-CCD mode, and the GIS was in the normal PH mode with the nominal bit assignments.

3. Analysis and Results

3.1. Upper Limits for L1157-mm and IRAS 20353+6742

Figure 1 shows GIS images in the soft (0.7 – 2.0 keV), and hard (2.0 – 10 keV) energy bands. The images are smoothed by a Gaussian function with a σ of 0.5'. The position of L1157-mm is shown with an open circle located about 6.5' (0.8 pc) east of the field center. There is no particular X-ray excess corresponding to L1157-mm in either GIS or SIS image. We calculated the upper limit of the X-ray emission from L1157-mm for the GIS data because systematic error of the SIS background was higher than that of the GIS. There are two different ways of background estimation. One is to take the symmetrical position of the source with respect to the optical axis, and the other is using the public GIS blank sky event data which are already corrected for point sources. The former is a reasonable method for background subtraction because the data are taken simultaneously, but the latter gives higher statistics.

As a result, both methods gave consistent results within the error at the 90% confidence level. The upper limit for the L1157-mm intensity at the 95% confidence is estimated to be $1.4 \times 10^{-3} \text{ c s}^{-1}$ in the 0.7 – 10 keV band, based on the combined data of GIS2 and GIS3 within a radius of $3'$ from the source position. Assuming a Raymond-Smith model with temperature $kT = 3.0 \text{ keV}$, metal abundance $Z = 0.3$, and $N_{\text{H}} = 1 \times 10^{21-24} \text{ cm}^{-2}$, the 95 % upper limit of the N_{H} corrected luminosity in a 0.5–10 keV band is estimated to be $1 \times 10^{30} - 2 \times 10^{32} \text{ erg s}^{-1}$ assuming the distance to be 440 pc as shown in table 1.

The ROSAT All Sky Survey (RASS) observation covered this region in Jan 8–18, 1991, with an exposure of 877 s and showed no significant X-ray emission. The upper-limit intensity in the energy range 0.1–2.0 keV is 0.02 c s^{-1} at the 3σ confidence level.

The Class I protostar in the L1152 dark cloud, IRAS 20353+6742, was located in the southwest direction in the GIS field of view (indicated by an open circle in figure 1), but the source again showed no significant X-ray emission. Although the source position falls on the built-in calibration source (^{55}Fe) in GIS3, and also close to the edge of the GIS field of view, we tried to estimate the upper limit of the luminosity of IRAS 20353+6742 in a similar way as for L1157-mm (table 1). The upper limit luminosity is about three times higher than that of L1157-mm because of the large offset angle.

3.2. Other Sources

Besides the non detection of L1157-mm and IRAS 20353+6742, several X-ray sources are clearly seen in figure 1. We performed a sliding cell method to pick up the sources. The cell size was $3' \times 3'$ (close to half power diameter of the XRT $\sim 3'$), and the soft(0.7–2.0 keV) and hard(2–10 keV) band images were separately examined. We set a 5σ threshold for the intensity in the a circle of $3'$ diameter, and 9 sources were significantly detected and listed in table 2. This table shows the significance for a diameter of $3'$ which contains about 50% of the photons from a point source.

Among the 9 sources, 3 objects (#6, #8, and #9) are detected in both energy bands, and 6 objects are detected in either soft or hard band only. Sources #2, #3, and #4 are soft-band detection, and #1, #5, and #7 are hard-band detection, respectively. Four sources, #1, #4, #6, and #9, have no cataloged counterpart in NED, SIMBAD database, and TYCHO catalog(Egret et al. 1992) within our position accuracy, $r < 1'$, and they are considered as new detections. We will call them as AXJ 2035+6806 (#1), AXJ 2036+6800 (#4), AXJ 2038+6801 (#6), and AXJ

2041+6800 (#9), respectively. Three sources, #2, #3, and #8, were already detected in RASS observation, and #2 and #8 have been identified as BWE 2034+6753 and HD 197471, respectively, within the position error of the ROSAT PSPC. The remaining two sources, #5 and #7, are difficult to judge whether they are really X-ray sources because of the poor statistics. We note that the source #5 is close to NGC 7023 SKCM 11; a star of spectral type F2V at a distance of 240 pc (Straizys et al. 1992). X-ray properties of the detected sources excluding #5 and #7 are described below.

#1, and #2, #3 — AXJ 2035+6806 and RASS sources

The position of source #1 is between #2 and #3 which are detected in the RASS observation, and the offset angles from these sources are 2.1' and 2.5', respectively. The position of #2 is in agreement with the coordinate of BWE 2034+6753. Since these 2 sources are not detected in the GIS hard band, their spectra are thought to be considerably soft. However, the poor statistics and the coupling with #1 hamper detailed spectral study of these sources. In contrast, source #1 emits X-rays only in the hard energy band. The fluxes of #1, #2, and #3 in table 2 could be overestimated because of the mutual flux contamination.

#4 — AXJ 2036+6800

This source is detected at 9' west from the field center. The coordinate is (R.A., Decl.)_{J2000} = (20^h36^m26^s, 68°0'11'') as determined from the center of gravity in the GIS image. The general accuracy of the position determination with ASCA has been studied for SIS data, which give better position resolution than GIS ones. The accuracy with the SIS is 40'' at the 90% confidence level (Gotthelf 1996), which is mostly determined by the systematic error in the satellite attitude calculation. Considering the GIS pixel size of 15'', the positional accuracy of the new source is estimated to be $\sim 1'$. The RASS observation did not indicate significant X-ray emission at this coordinate.

This source is rather faint and very soft in contrast to the next AXJ 2038+6801. The GIS hard-band image (figure 1(b)) shows no X-ray emission at the peak position of the soft-band image (figure 1(a)). Figure 2(a) shows the background-subtracted spectrum for the combined GIS2 and GIS3 data fitted with an absorbed thermal bremsstrahlung model. The GIS blank sky data are used as the background. The best-fit spectral parameters are $kT = 0.27^{+0.47}_{-0.14}$ keV, $N_{\text{H}} = 1.1^{+11}_{-1.1} \times 10^{21}$ cm⁻² (the error shows 90 % confidence level) shown in table 3, and the

absorbed flux in 0.5–2.0 keV band is $\sim 1 \times 10^{-13}$ erg cm $^{-2}$ s $^{-1}$. The closest object to this source is a star BD+67 1258 which is identified as NGC 7023 SCKM 8; a G0IV star with $m_V \sim 10.30$, at a distance of 180 pc (Straizys et al. 1992). The angular distance of this candidate star, 1.2', is slightly larger than the positional error.

#6 — AXJ 2038+6801

AXJ 2038+6801 is clearly detected in the center of the GIS image as shown with a filled triangle in figure 1. The spatial extent of the source is consistent with the XRT point spread function. The coordinate is (R.A., Decl.) $_{J2000} = (20^{\text{h}}37^{\text{m}}59^{\text{s}}, 68^{\circ}1'2'')$, and the position accuracy is estimated to be the same as the previous case, i.e. $\sim 1'$. Again, there is no X-ray emission in the RASS observation. The counting rate in the 0.5–10 keV band is 0.015 c s $^{-1}$ for the sum of GIS2 and GIS3 within a radius of 6'.

The spectrum is shown in figure 2(b) fitted with an absorbed power-law model. Spectral models for thermal bremsstrahlung and power-law emission are both acceptable with appropriate absorption. The resultant parameters are shown in table 3. The bremsstrahlung fit gives a temperature $kT = 7.6^{+16}_{-3.5}$ keV, and the power-law model indicates a photon index to be 2.0 ± 0.5 . For both models, the observed 0.5–10 keV flux is 5.8×10^{-13} erg cm $^{-2}$ s $^{-1}$ and the absorption column density N_{H} is as large as 2×10^{22} cm $^{-2}$ which is significantly larger than the Galactic interstellar absorption of 1.4×10^{21} cm $^{-2}$ based on the 21cm line measurement (Dickey, Lockman 1990). The absorbed GIS spectrum predicts a PSPC count rate of 0.0025 c s $^{-1}$, which is lower than the actual 3σ upper limit (0.02 c s $^{-1}$) for this position. It is, therefore, natural that the source is undetected with PSPC. We added a Gaussian line to the thermal bremsstrahlung model at a center energy of 6.4 and 6.7 keV assuming a neutral and He-like iron-K line, respectively. The upper limit of the equivalent width is 708 eV (6.4 keV line) and 1020 eV (6.7 keV line) at the 95% confidence level, respectively.

We also performed time variability analysis to search for flare like events or pulsations. The light curve shows no significant variability during the total observation interval ~ 100 ks. The highest counting rate for a bin size of an hour is about twice the average, which is typically 207 counts for the sum of GIS2 and GIS3 within a circle of $r = 6'$ in 0.5–10 keV and dominated by the source flux. Also, a power spectrum obtained from an FFT analysis (Leahy et al. 1983) does not show any significant peak above the 99% confidence level over a frequency range 3.9×10^{-5} Hz – 16 Hz. The largest power appears at a frequency 1.4 Hz, and the upper limit for a relative amplitude is 49% of the intensity at the 99% confidence level assuming a sinusoidal pulse shape.

#8 — HD 197471

The peak position of this source is consistent with that of HD 197471 within about $0.5'$, which is also identified as NGC 7023 SCKM 23; a star with a spectral type F7V at a distance of 94 pc (Straizys et al. 1992). The RASS data shows an X-ray source at the same position. Figure 2(c) shows the observed GIS spectrum fitted with an absorbed thermal bremsstrahlung model. The best-fit spectral parameters are $kT = 0.66_{-0.44}^{+1.4}$ keV, $N_{\text{H}} = 1.2_{-1.0}^{+2.6} \times 10^{22}$ cm $^{-2}$ (the error shows the 90 % confidence level), and the absorbed flux in 0.5–2.0 keV band is $\sim 2 \times 10^{-13}$ erg cm $^{-2}$ s $^{-1}$. The absorption corrected luminosity is estimated to be 1.2×10^{30} erg s $^{-1}$ for the distance of 94 pc. The positional consistency suggests that this source is the star HD 197471, emitting a spectrum with $kT \sim 0.7$ keV.

#9 — AXJ 2041+6800

This source is not identified, and no corresponding source is seen in the RASS data. The observed spectrum is shown in figure 2(d) fitted with an absorbed power-law model including a gaussian line. The 0.5–10 keV flux is $\sim 4 \times 10^{-13}$ erg cm $^{-2}$ s $^{-1}$. The reduced χ^2 value improves by the inclusion of a gaussian line with an equivalent width $EW = 1.9$ keV in the absorbed power-law model (from 1.17 to 0.99) as shown in table 3. The reduction of $\Delta\chi^2 = 5.5$ with the decreased degrees of freedom of 2 indicates that the line is significant at the 90% confidence level (Malina et al. 1976). The best-fit value of the line center energy is ~ 4.6 keV, so that the implied redshift is ~ 0.4 assuming that the line is either neutral or He-like iron-K line. Taking this redshift and assuming $q_0 = 0.5$, the 0.5–10 keV luminosity at the source is estimated to be $1.2 \times 10^{44} h^{-2}$ erg s $^{-1}$, where $h = H_0/100$ km s $^{-1}$ Mpc $^{-1}$ is the dimensionless Hubble constant. We also fit the spectrum with an absorbed Raymond–Smith model. The best-fit parameters are temperature of $kT \sim 5.4$ keV, metal abundance of $Z \sim 2.2$ solar, and redshift of $z \sim 0.39$, respectively, as shown in table 3. Therefore, an unusually high metal abundance is implied if the emission line is real.

4. Discussion

The upper limit we have obtained for the X-ray luminosity of L1157-mm, 10^{30-32} erg s $^{-1}$, is comparable to or less than those of Class I objects, such as WL6 and EL29 in the ρ Ophiuchi dark cloud (Kamata et al. 1997). The Class I protostar in the L1152 dark cloud, IRAS 20353+6742, showed no significant X-ray emission, either.

The X-ray luminosities of the Class I objects so far studied do not show clear correlation with physical parameters

such as M_{env} , L_{bol} , and F_{CO} . A relative configuration between the direction of the CO bipolar outflow and the line of sight is suggested as a relevant parameter. For IRAS 20353+6742, both L_{bol} ($= 3.3L_{\odot}$) and M_{env} ($= 0.05M_{\odot}$) take intermediate values between those for WL6 ($L_{\text{bol}} = 2.0L_{\odot}$ and $M_{\text{env}} = 0.02M_{\odot}$) and EL29 ($L_{\text{bol}} = 41.0L_{\odot}$ and $M_{\text{env}} = 0.09M_{\odot}$; Bontemps et al. 1996). In the ρ Ophiuchi dark cloud, all the inclination angles of X-ray emitting protostars are less than 30° (Sekimoto et al. 1997). In contrast, the CO outflow of L1152 shows almost an edge-on configuration (Bontemps et al. 1996). Since an absorbing gas with $N_{\text{H}} \gtrsim 10^{23} \text{ cm}^{-2}$ can hide an object with $L_{\text{X}} \sim 10^{31} \text{ erg s}^{-1}$ as indicated in table 1, the present negative result for IRAS 20353+6742 can be understood in terms of a geometrical effect.

So far, no significant X-ray emission from Class 0 protostars has been detected including L1157-mm. We may consider three possible causes of the low X-ray luminosity of Class 0 objects: 1) intrinsic low activity for the X-ray emission in this class, 2) absorption by thick surrounding gas or dust, 3) some effect due to source configuration. In the first case, Class 0 objects are in the evolutionary stage where the X-ray emission has not started yet. In the second case, the thick disk component ($N_{\text{H}} > 10^{23-24} \text{ cm}^{-2}$) hampers X-ray detection of an object with $L_{\text{X}} \sim 10^{31} \text{ erg s}^{-1}$ in the present energy range (see table 1). In fact the envelope mass of L1157-mm ($\sim 3M_{\odot}$) is significantly larger than those of WL6 and EL29, and the envelope is supposed to extend around the core. In the last case, the lack of clear X-ray emission from L1157-mm can be understood because the inclination angle of CO outflow is $\sim 80^{\circ}$, i.e. an almost edge-on configuration, assuming that the X-ray emission of protostars is collimated parallel to the CO outflow. If this is the case, there remains a possibility for detecting X-ray emission from Class 0 protostars for which outflows are looked at in the exactly pole-on configuration (with an inclination angle of $0 \pm 10^{\circ}$), even if the envelope mass is larger than those of Class I protostars.

The most luminous new X-ray source in the field, AXJ 2038+6801, shows a hard X-ray spectrum with strong absorption and no obvious time variability. Within $5'$ from the source, no identification is made with SIMBAD, NED database, and TYCHO catalog (Egret et al. 1992), which leaves various possibilities for the source nature. Assuming the distance of AXJ 2038+6801 to be the same as that of the L1157 cloud (440 pc), the 0.5–10 keV luminosity corrected for the absorption is estimated to be $\sim 2 \times 10^{31} \text{ erg s}^{-1}$. This is similar to the luminosity of X-ray luminous young stellar objects. The ratio of the X-ray measured N_{H} to the optically estimated A_{V} for L1157-mm (20 mag: Davis, Eisloffel 1995) suggests a relation $\sim 10^{21} \text{ cm}^{-2} \text{ mag}^{-1}$: which is consistent with those for X-ray luminous Class I objects. Hence, if L1157 dark cloud has a large spatial extent ($\sim 0.8 \text{ pc}$) and reaches the

position of AXJ 2038+6801, the observed strong absorption is naturally explained.

If AXJ 2038+6801 is not associated with L1157 and is located within our galaxy, the luminosity has to be roughly in the range $10^{31} - 10^{34}$ erg s⁻¹. Galactic X-ray binary sources containing neutron stars or black holes generally exhibit hard X-ray spectra, but their luminosities are mostly higher by orders of magnitude. White dwarf binaries and Crab-like pulsars have X-ray luminosities in this range and produce fairly hard spectra. The present negative detection of X-ray pulses suggest that the possibility for Crab-like pulsars is low unless the pulse frequency is faster than 16 Hz. Dwarf novae show X-ray luminosities in the range 10^{31-33} erg s⁻¹ and hard spectra with $kT \gtrsim 10$ keV. Only the lack of time variation is the different characteristics of AXJ 2038+6801 from dwarf novae. Therefore, this possibility remains as the nature of AXJ 2038+6801. The hard spectrum of this source also suggests a possibility of intrinsically absorbed or obscured AGN. Based on the $\log N - \log S$ relation (Ueda et al. 1999), it is expected that one or two serendipitous sources with this flux level ($\sim 5 \times 10^{-13}$ erg cm⁻² s⁻¹) are detected in the GIS field of view in a 60 ks observation.

Another new source AXJ 2036+6800 shows a significantly softer spectrum, with no detectable X-ray emission above 2 keV. The absorption is much weaker than the previous case of AXJ 2038+6801. Regarding its spectrum ($kT \sim 0.3$ keV), we will consider a possibility of a late type star. Assuming that the source has the same distance as the closest star BD+67 1258 (spectral type G0IV), the 0.5–2.0 keV luminosity becomes 8.0×10^{29} erg s⁻¹. This is in the higher end in the luminosity distribution of main-sequence (F and G type) stars with $kT \sim 0.3$ keV (Schmitt et al. 1990). It is, therefore, possible that the source can be a late-type star.

The spectrum of AXJ 2041+6800 shows an interesting feature which may be a redshifted iron line. A simple χ^2 test indicates that the line is significant at the 90% confidence as shown in the previous section. However, the line energy is close to the L-edge energy (4.78 keV) of Xe, which is the detector gas of the GIS instrument. We should be cautious about the detection of the strong iron line, and should wait for further observations with better statistics. If the redshift is really around 0.4, the implied luminosity indicates that the source is either an AGN or a cluster of galaxies.

Among the other detected sources, three have been detected with the RASS. One is identified to be an F type star, HD 197471, and its spectrum ($kT < 1$ keV) and luminosity (1.2×10^{30} erg s⁻¹ in 0.5–2.0 keV) are consistent with the emission from a late-type star. The other two sources are close to each other and confused with AXJ 2035+6806. Observations with higher angular resolution are needed to look into the nature of these sources.

The authors thank Y. Sekimoto, M. Umemoto for providing the recent radio observation results, S. Sasaki for discussion, and Y. Ishisaki, K. Kikuchi, and Y. Ueda for helping the data analysis. We also thank the anonymous referee for useful comments and suggestions. NASA/IPAC Extragalactic Database (NED) is operated by Jet Propulsion Laboratory, Caltech, under contract with NASA and the SIMBAD data base is operated by the Centre de Données astronomiques de Strasbourg.

References

- André P., Ward-Thompson D., Barsony M. 1993, *ApJ* 406, 122
- Bachiller R. 1996, *ARA&A* 34, 111
- Bontemps S., André P., Terebey S., Cabrit S. 1996, *A&A* 311, 858
- Burke B.E., Mountain R.W., Harrison D.C., Baults M.W., Doty J.P., Ricker G.R., Daniels P.J. 1991, *IEEE Trans.*, ED-38, 1069
- Casanova S., Montmerle T., Feigelson E.D., André P. 1995, *ApJ* 439, 752
- Davis C.J., Eislöffel J. 1995, *A&A* 300, 851
- Dickey J.M., Lockman F.J. 1990, *Ann. Rev. Ast. Astr.* 28, 215
- Egret D., Didelon P., McLean B.J., Russell J.L., Turon C. 1992, *A&A* 258, 217
- Gotthelf E. 1996, *ASCA News* 4, 31
- Gueth F., Guilloteau S., Dutrey A., Bachiller R. 1997, *A&A* 323, 943
- Kamata Y., Koyama K., Tsuboi Y., Yamauchi S. 1997, *PASJ* 49, 461
- Koyama K., Hamaguchi K., Ueno S., Kobayashi N., Feigelson E.D. 1996, *PASJ* 48, L87
- Leahy D.A., Darbro W., Elsner R.F., Weisskopf M.C., Sutherland P.G., Kahn S., Grindlay J.E. 1983, *ApJ* 266, 160
- Malina R., Lampton M., Bowyer S. 1976, *ApJ* 209, 678
- Myers P.C., Fuller G.A., Mathieu R.D., Beichman C.A., Benson P.J., Schild R.E., Emerson J.P. 1987, *ApJ* 319, 340
- Ohashi T., Ebisawa K., Fukazawa Y., Hiyoshi K., Horii M., Ikebe Y., Ikeda H., Inoue H. et al. 1996, *PASJ* 48, 157
- Ozawa H., Nagase F., Ueda Y., Dotani T., Ishida M. 1999, *ApJ* 523, L81
- Sekimoto Y., Tatematsu K., Umemoto T., Koyama K., Tsuboi Y., Hirano N., Yamamoto S. 1997, *ApJ* 489, L63
- Schmitt J.H.M.M., Collura A., Sciortino S., Vaiana G.S., Harnden F.R. Jr, Rosner R. 1990, *ApJ* 365, 704
- Straižys V., Černis K., Kazlauskas A., Meištās E. 1992, *Baltic Astronomy* 1, 149

Tafalla M., Bachiller R. 1995, ApJ 443, L37

Tanaka Y., Inoue H., Holt S.S. 1994, PASJ 46, L37

Ueda Y., Takahashi T., Inoue H., Tsuru T., Sakano M., Ishisaki Y., Ogasaka Y., Makishima K., Yamada T., Akiyama M., Ohta K. 1999, ApJ 518, 656

Umemoto T., Iwata T., Fukui Y., Mikami H., Yamamoto S., Kameya O., Hirano N. 1992, ApJ 392, L83

Table 1. The 95%-confidence upper limit for the X-ray luminosity of L1157-mm and IRAS 20353+6742 after correction for the absorption in the energy band 0.5–10 keV.

N_{H} (cm^{-2})	L_{x} (0.5–10 keV) ($10^{31} \text{ erg s}^{-1}$)	L_{x} (0.5–10 keV) ($10^{31} \text{ erg s}^{-1}$)
	L1157-mm	IRAS 20353+6742
1×10^{21}	< 0.13	< 0.39
1×10^{22}	< 0.22	< 0.67
1×10^{23}	< 1.1	< 3.5
1×10^{24}	< 20	< 77

Table 2. The source list detected in the GIS field with more than 5σ significance. Sources #6, #8, and #9 are detected in both soft (0.7–2.0 keV) and hard (2.0–10 keV) energy bands. Sources #2, #3, and #4 are detected in the soft band only, and #1, #5, and #7 are in the hard band only.

No.	R.A.	Decl.	Significance (σ)*		F_X (0.5–10 keV) (10^{-13} erg cm $^{-2}$ s $^{-1}$)	ID †
	J2000	J2000	soft	hard		
#1	20 ^h 35 ^m 19 ^s	68°06′19″	4.70	7.35	3.7	not available (AXJ 2035+6806)
#2	20 ^h 35 ^m 25 ^s	68°04′51″	5.54	4.19	3.8	BWE 2034+6753, RASS source
#3	20 ^h 35 ^m 33 ^s	68°07′34″	7.05	4.08	3.8	RASS source
#4	20 ^h 36 ^m 26 ^s	68°00′11″	7.49	2.71	1.0	BD+67 1258 ? (AXJ 2036+6800)
#5	20 ^h 37 ^m 34 ^s	67°55′06″	2.15	5.89	0.5	NGC 7023 SCKM 11
#6	20 ^h 37 ^m 59 ^s	68°01′02″	10.0	21.9	5.8	not available (AXJ 2038+6801)
#7	20 ^h 38 ^m 55 ^s	68°07′22″	1.93	5.35	1.4	not available
#8	20 ^h 40 ^m 02 ^s	67°47′56″	10.5	5.53	2.0	HD 197471, RASS source
#9	20 ^h 41 ^m 04 ^s	68°00′09″	8.02	6.43	3.5	not available (AXJ 2041+6800)

* Estimated within a diameter of 3′.

† Names in parentheses are used in the text.

Table 3. Spectral parameters for source #4, #6, #8, and #9. The errors are statistical and 90%-confidence levels for single parameter of interest.

	Target name	Model	N_H (10^{22} cm^{-2})	Γ/kT (/keV)	EW^\dagger/Z^\ddagger (keV/solar)	$\chi^2/d.o.f$
#4	AXJ 2036+6800	Bremsstrahlung*	$0.11^{+1.1}_{-0.11}$	$0.27^{+0.47}_{-0.14}$		5.14/10
#6	AXJ 2038+6801	Power law*	$2.3^{+1.1}_{-1.0}$	$2.0^{+0.5}_{-0.5}$		23.9/22
		Bremsstrahlung	$1.9^{+0.8}_{-0.7}$	$7.6^{+16}_{-3.5}$		23.4/22
#8	HD 197471	Bremsstrahlung*	$1.2^{+2.6}_{-1.0}$	$0.66^{+1.4}_{-0.44}$		5.03/8
#9	AXJ 2041+6800	Power law	$0.61^{+2.7}_{-0.61}$	$1.7^{+1.6}_{-0.78}$		23.4/20
		Power law + Gaussian*	$0.85^{+3.0}_{-0.85}$	$2.2^{+1.8}_{-1.0}$	$1.9^{+1.5}_{-1.3} \dagger$	17.9/18
		Raymond-Smith	$0.68^{+2.1}_{-0.68}$	$5.4^{+6.7}_{-2.6}$	$2.2^{+2.8}_{-1.9} \ddagger$	21.1/21

* Models fitted to the data in figure 2.

† Equivalent width.

‡ Metal abundance.

Fig. 1. The GIS image in two energy bands: 0.7–2.0 keV (a), and 2.0–10 keV (b). Dashed circles show L1157 and L1152 regions with a radius of $2'$, which roughly corresponds to the size of CO outflows. Filled triangles indicate positions of nine new X-ray sources detected in the GIS field (see table 2). Filled squares show positions of identified objects, BWE 2034+6753 (radio source), BD+67 1258 (star), NGC 7023 SCKM 11 (star), and HD 197471(star) for sources #2, #4, #5, and #8, respectively. The surrounding dotted circle shows the effective field of view of GIS : $r = 20'$.

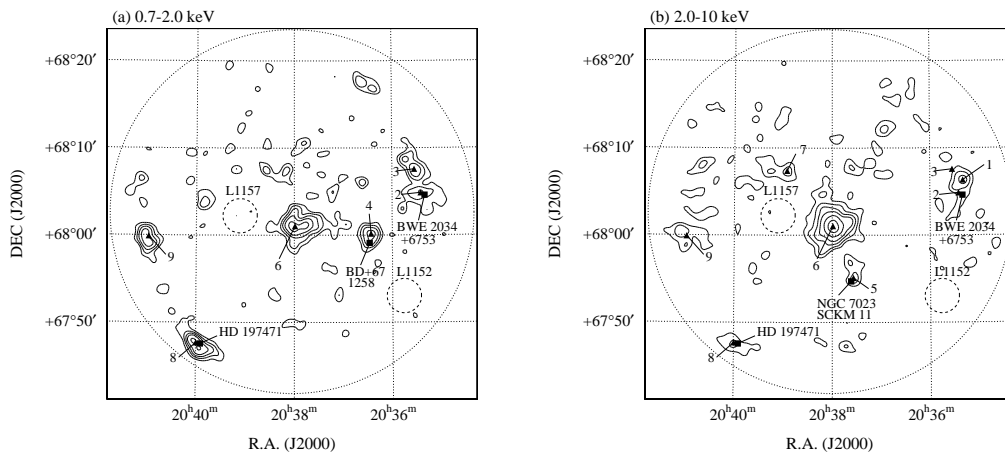


Fig. 2. Spectra with GIS2 and 3 of new X-ray sources AXJ 2036+6800(a), AXJ 2038+6801(b), HD 197471(c), and AXJ 2041+6800(d). The models fitted to the data are indicated with asterisks in table 3. The bottom panels show residuals of the fits in units of standard deviation.

